Kinetic model of local droplet etching

Christian Heyn

Institut für Angewandte Physik und Zentrum für Mikrostrukturforschung, Jungiusstraße 11, D-20355 Hamburg, Germany

The self-organized *in situ* drilling of nanoholes into semiconductor surfaces by using liquid metallic droplets during conventional molecular beam epitaxy represents a new degree of freedom for the design of heterostructure devices. A model of this local droplet etching is presented that is based on a core-shell droplet structure. With the model, the evolution of the droplet and substrate morphology is calculated. We demonstrate quantitative agreement between model results and measured morphologies. Furthermore, also the influence of the process temperature is correctly reproduced by the model.

I. INTRODUCTION

The functionalization of metallic droplets during semiconductor epitaxy represents a very promising new degree of freedom for the design of novel types of nanostructures. A prominent example is the droplet epitaxy[1–10] which by droplet crystallization generates semiconductor quantum dots (QDs),[3–7] QD molecules,[8] or quantum ring complexes.[9,10] Examples of Ga droplets and of droplet epitaxial GaAs QDs generated on AlGaAs surfaces over a wide range of growth temperatures are shown in Fig. 1. At high temperatures, the droplets act as an etchant performing a self-organized drilling of deep nanoholes into semiconductor surfaces. This local droplet etching (LDE) occurs during postgrowth annealing[11] and was first demonstrated by Wang *et al.*[12] for the etching of GaAs surfaces with Ga droplets. Later, the range of materials was expanded and etching was performed with Ga (Refs. 11–13), Al (Refs. 14–16), and InGa (Refs. 17 and 18) droplets on GaAs (Ref. 12), AlGaAs (Refs. 11, 13, 17, and 18), and AlAs (Refs. 14–16) surfaces. An example of an AlGaAs surface with LDE nanoholes is shown in Fig. 2(a).

LDE is fully compatible with conventional molecular beam epitaxy (MBE) technology and allows the integration of maskless spacially limited etching processes into MBE growth of semiconductor heterostructures. A first application of the LDE nanoholes is their use as a self-organized template for the nucleation of low dense InAs QDs with controlled optical properties.[19] We have demonstrated recently that the filling of nanoholes yields strain-free GaAs QDs which depend on the process conditions being either highly uniform[14,16] or show broadband optical emission.[15,16]

As a further important point, similar to nanovulcanos, the nanoholes are surrounded by distinct walls [Fig. 2(a)] crystallized from droplet material and As from the substrate.[13,17,18] Depending on the choice of the droplet material, the walls either provide a quantum-ring confinement (GaAs in AlGaAs, Refs. 13 and 17) or behave like an isolator (AlAs, Refs. 14–16).

So far, only very few studies on the basic physics of metallic droplets during semiconductor epitaxy have been presented. Important recent findings include, for instance, the relevance of Ostwald ripening during droplet nucleation,[5] droplet running,[20] and the formation of a core-shell droplet structure.[21] In this field, the combined hole drilling and wall formation during LDE represents a fascinating point, that is, that the same droplet performs two opposite operations: First,

the removal of material from the substrate which results in nanohole formation and second, the deposition of material on the substrate as wall surrounding the nanohole opening.

We present here experimental results on the nanohole morphology together with a kinetic model that explains the basic mechanism behind droplet etching. In particular, we discuss etching of (001) GaAs or AlGaAs surfaces with Ga droplets as a model system. Previous studies reveal that droplet nucleation[5] and hole etching[13,14] do not significantly depend on the choice of either GaAs or AlGaAs as substrate. As a central assumption, the model considers that a droplet is build of a liquid Ga core which is covered by a thin GaAs shell. The liquid core in contact with the substrate results in drilling and the shell in deposition of the wall.

II. EXPERIMENTAL PROCEDURE

The nanohole samples were fabricated on (001) GaAs wafers using solid-source molecular beam epitaxy with a valved cracker cell for As_4 supply. After surface oxide desoption, an GaAs or AlGaAs buffer was grown. Etching on both substrate materials yields nanoholes with nearly identical structural properties. For droplet etching, the As valve and shutter were closed and the sample was heated to a temperature T. Droplets were generated on the substrate surface in Volmer-Weber growth mode by deposition of only Ga at a flux corresponding to a GaAs growth speed of $F = 0.8$ monolayers (ML)/s. The Ga coverage θ was adjusted by varying the deposition time. After doplet generation, a postgrowth annealing step of $t = 180$ s was applied. During this annealing step, the transformation of the initial droplets into nanoholes with wall takes place. The surface morphology was inspected with atomic force microscopy (AFM) in tapping mode.

III. DROPLET DENSITY AND VOLUME

Directly after deposition ($t = 0$ s) the droplets are composed of pure Ga, where t is the annealing time. The average number of Ga atoms inside a droplet is $N_0 = (\theta - 1)/(n/n_{\rm Surf})$, with the deposited Ga coverage θ, the droplet density n, and the density $n_{\rm Surf} = 6.25 \times 10^{14}$ cm^{-2} of GaAs surface sites. This approach considers that the first monolayer Ga will be consumed for the transition from an As terminated into a Ga terminated surface structure.[5,11] The value of N_0 defines the
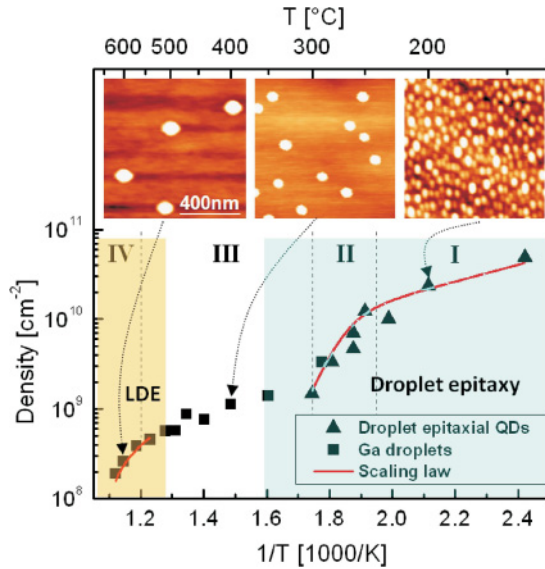
FIG. 1. (Color online) Symbols: measured density n of Ga droplets and of GaAs QDs (from Ref. [5]) on (001) AlGaAs vs. T. The GaAs QDs result from droplet crystallization under As atmosphere and their density is equal to the density of the initial droplets.[5] Lines: calculated droplet density as is described in the text. The Ga coverage was $\theta = 3.2$ ML and the growth speed $F = 0.8$ ML/s. Four regimes, I, II, III, and IV, are distinguished depending on the slope of the n vs. T dependence. The yellow colored area marks the temperature regime used for droplet etching and blue the droplet epitaxy regime. The inset on top shows typical AFM images from corresponding surfaces.

initial droplet size in the model and represents the number of atoms that must be removed for hole formation.

The droplet density n is an important quantity for the calculation of N_0. Measured values of n vs. T at a constant coverage $\theta = 3.2$ ML are plotted in Fig. 1. A scaling law quantitatively reproduces the experimental n in the droplet epitaxy regimes I and II.[5] After adjustment of the parameters,[11] the scaling law is used here for the calculation of the droplet density in the LDE regime IV: $n(t = 0) = j \exp[E_N/(k_B T)](1 + t_r/\tau_r)^{-1}$, with the constant $j = 2 \times 10^5$ cm^{-2}, the characteristic energy $E_N = 0.54$ eV, Boltzmann's constant k_B, the temperature T, $t_r = 20$ s, the characteristic time[5] $\tau_r = \nu^{-1} \exp[E_r/(k_B T)]$, the vibrational frequency[22] $\nu = 2k_B T/h$, Planck's constant h, and $E_r = 2.68$ eV. A comparison of results calculated with the
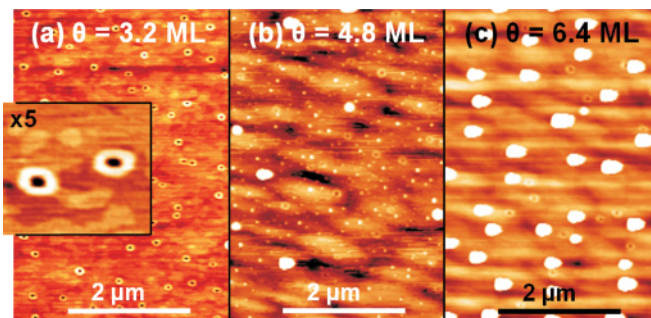

FIG. 2. (Color online) AFM images of (001) AlGaAs surfaces after LDE with Ga droplets at a coverage θ of (a) 3.2 ML, (b) 4.8 ML, and (c) 6.4 ML. The temperature during the LDE process was $T = 570\,^\circ$C and the postgrowth annealing time 180 s.

scaling law and experimental values in the LDE regime IV is shown in Fig. 1.

IV. DROPLET MATERIAL REMOVAL

For the transformation of the droplets into nanoholes, the droplet material must be removed from the initial droplet position during a post-growth annealing step.[11] Figure 2 shows AFM images of AlGaAs surfaces after LDE with Ga droplets. Different Ga coverages $\theta = 3.2$, 4.6, and 6.4 ML were studied. For $\theta = 6.4$ ML, we find nanoholes and, in addition, a high density of very large clusters. This observation indicates that at high θ the droplet material has not completely desorbed. Instead of that, coalescence and coarsening by Ostwald ripening[24] causes the formation of large clusters. On the other hand, at $\theta = 3.2$ ML, only very few large clusters are visible and the surface morphology between the holes is nearly atomically flat. From this result we conclude that desorption is the central mechanism for droplet material removal at low θ. Since the existence of large clusters is unfavorable for most applications of the LDE technique, we focus in the present model of the droplet etching process on the low coverage case and consider Ga desorption from the droplet surface as main process for droplet material removal.

V. DROPLET GEOMETRY

The initial configuration of our model considers a flat (001) GaAs surface on which a pure Ga droplet has been generated. During the annealing step, the GaAs shell formation takes place and the time-dependent volume of the droplet is the sum of the liquid Ga core volume $V_{\text{Core}} = V_{\text{Ga}} N_{\text{Ga,Core}}$ plus the GaAs shell volume $V_{\text{Shell}} = V_{\text{GaAs}} N_{\text{Ga,Shell}}$, with the numbers $N_{\text{Ga,Core}}$ and $N_{\text{Ga,Shell}}$ of Ga atoms inside the droplet core and shell. We distinguish between the atomistic volume $V_{\text{Ga}} = (V_{\text{mol}}/N_{\text{Avo}}) = 1.96 \times 10^{-29}$ m^3 of a Ga atom inside the liquid Ga core and the volume $V_{\text{GaAs}} = a_0^3/4 = 4.52 \times 10^{-29}$ m^3 of a GaAs molecule inside the GaAs shell, with the mol volume V_{mol} of Ga, Avogadro's constant N_{Avo}, and the GaAs lattice constant a_0.

According to a previous publication,[17] we assume that the droplet core is shaped like a segment of a sphere, with height $h_{\text{Core}} = (V_{\text{Core}}/[(\pi/6)(3/\alpha^2 + 1)])^{1/3}$, and radius $r_{\text{Core}} = h_{\text{Core}}/\alpha$. The value of the constant $\alpha = 0.35$ is taken from AFM measurements. The height of the shell is $h_{\text{Shell}} = ([V_{\text{Core}} + V_{\text{Shell}}]/[(\pi/6)(3/\alpha^2 + 1)])^{1/3}$ and the shell radius $r_{\text{Shell}} = h_{\text{Shell}}/\alpha$. For instance, deposition at $T = 570\,^\circ$C and $\theta = 3.2$ ML yields droplets with $n = 3.2 \times 10^8$ cm^{-2}, $N_{\text{Ga,Core}}(t = 0) = N_0 = 4.3 \times 10^6$ atoms, and $r_{\text{Core}} = 53$ nm.

VI. BASIC MODEL ASSUMPTIONS

An overview on the droplet geometry and the relevant processes is shown in Fig. 3. As the starting point for our model of the local droplet etching we consider a typical Ga droplet on a flat GaAs surface. The number of atoms N_0 inside this droplet is calculated from the deposited Ga coverage θ and the droplet density n, as is described in Sec. III. According to Sec. III, this allows the calculation of the droplet structural parameters (i.e., the radius and surface area). During annealing, the removal
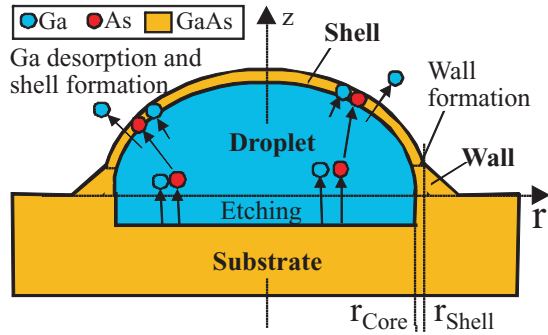
FIG. 3. (Color online) Scheme of the droplet geometry and the processes considered in the core-shell model.

of the droplet material takes place via desorption from the droplet surface as is discussed in Sec. IV. The corresponding rate at which a single Ga desorbs from the droplet surface is $R_D = \nu \exp[-E_D/(k_B T)]$, with the activation energy E_D. Obviously, desorption reduces the number of Ga atoms inside the droplet. The corresponding time evolution of $N_{Ga,Core}$ is calculated using a kinetic rate equation as will be discussed below.

The central process for etching is diffusion of As atoms from the substrate into the liquid droplet core driven by the concentration gradient. The corresponding etching rate is $R_E = (x_{As,max} - x_{As})\nu \exp[-E_E/(k_B T)]$ for $x_{As} < x_{As,max}$ and $R_E = 0$ for $x_{As} \geqslant x_{As,max}$, with the maximum solubility $x_{As,max}$ of As in liquid Ga, the As concentration $x_{As} = N_{As,Core}/(N_{Ga,Core} + N_{As,Core})$, the number $N_{As,Core}$ of As atoms inside the droplet core, and the activation energy E_E. From data reported by Thurmond,[23] we estimate the temperature dependent maximum solubility $x_{As,max} = 6.1 \times 10^{-10} \exp(T[K]/60)$ of As in liquid Ga. This yields for instance at $T = 570\,^{\circ}\mathrm{C}$ a very low $x_{As,max}$ of 8×10^{-4}. The removal of As causes the liquefaction of the substrate at the interface to the droplet. On the other hand, the additional As increases x_{As} inside the droplet and due to the limited $x_{As,max}$ etching would quickly stop without an additional mechanism reducing the As concentration.

We assume that shell and wall formation represent this mechanism allowing etching to proceed. The process is as follows: desorption of only Ga from the droplet surface causes a local increase of the As concentration which there exceeds the maximum solubility. As a result, GaAs is precipitated and is assumed to form a thin GaAs shell surrounding the liquid droplet core. This approach illuminates an important difference between the droplet/substrate interface and the droplet surface. Since droplet material removal by Ga desorption takes place only at the droplet surface, the As concentration is locally increased only there. That means, the low As concentration inside the droplet yields etching at the droplet/substrate interface and the high As concentration at the droplet surface results in shell formation. In other words, there is a diffusion flux of As from the substrate to the shell. The existence of a core-shell configuration has already been observed for In droplets on GaAs (Ref. 21). The rate at which Ga and excessive As from the droplet core precipitate into the GaAs shell is $R_S = x_{As}\nu \exp[-E_S/(k_B T)]$, where E_S is an activation energy.

As the last process, GaAs from the shell is deposited at the shell/substrate interface and crystallizes as the wall which surrounds the nanohole opening. The corresponding rate is $R_C = \nu \exp[-E_C/(k_B T)]$, with activation energy E_C.

VII. RATE MODEL OF DROPLET ETCHING

The dynamic evolution of the droplet size and the surface morphology is described by two sets of kinetic rate equations. Set 1 with Eqs. (1)...(3) characterizes the time-dependent numbers of Ga and As atoms inside the droplet core and shell. These numbers are modified by the processes of etching, desorption, shell formation, and wall deposition. From the number of atoms inside the droplet core, the time-dependent droplet volume and radius are calculated. The number of atoms inside the shell gives the time-dependent shell volume and radius. The second set of equations with Eqs. (4) and (5) is used to calculate the surface morphology evolution. Equation (4) is valid at the interface between droplet core and substrate and describes the etching of substrate material below the droplet. Equation (5) is valid at the interface between shell and substrate and reflects the deposition of material forming the wall. Thus, the time-dependent radii do not enter Eqs. (4) and (5) directly, but they define the part of the surface area at which the respective equation is valid.

The following set of three, Eqs. (1) through (3), characterize the time-dependent numbers of Ga and As atoms inside the droplet core and shell. First, the number of Ga atoms inside the droplet is calculated, which is influenced by desorption, etching, and shell formation

$$\frac{d}{dt}N_{Ga,Core} = -\left(S_{Core}/V_{Ga}^{2/3}\right)R_D + \left(A_{Core}/V_{GaAs}^{2/3}\right)R_E - \left(S_{Core}/V_{Ga}^{2/3}\right)R_S, \quad (1)$$

with the droplet core surface area S_{Core} and the contact area A_{Core} between droplet core and substrate. The number of As atoms inside the droplet is influenced by etching and shell formation

$$\frac{d}{dt}N_{As,Core} = \left(A_{Core}/V_{GaAs}^{2/3}\right)R_E - \left(S_{Core}/V_{Ga}^{2/3}\right)R_S. \quad (2)$$

The GaAs shell is composed of equal numbers of Ga and As atoms ($N_{Shell} = N_{Ga,Shell} = N_{As,Shell}$) that are modified by shell formation and wall deposition

$$\frac{d}{dt}N_{Shell} = \left(S_{Core}/V_{Ga}^{2/3}\right)R_S - \left(A_{Shell}/V_{GaAs}^{2/3}\right)R_C, \quad (3)$$

with the contact area A_{Shell} between droplet shell and substrate.

The second set of two equations (4) and (5) is used to calculate the surface morphology evolution $z(r,t)$, where $r = 0$ is the center of the projection of the droplet onto the surface. The starting point is a flat surface with $z(r,0) = 0$. Etching takes place at the core/substrate interface ($r < r_{Core}$) and locally lowers the surface according to

$$\frac{d}{dt}z = -V_{GaAs}^{1/3}R_E. \quad (4)$$

The deposition of wall material takes place at the shell/substrate interface ($r_{Core} \leqslant r < r_{Shell}$) and locally raises
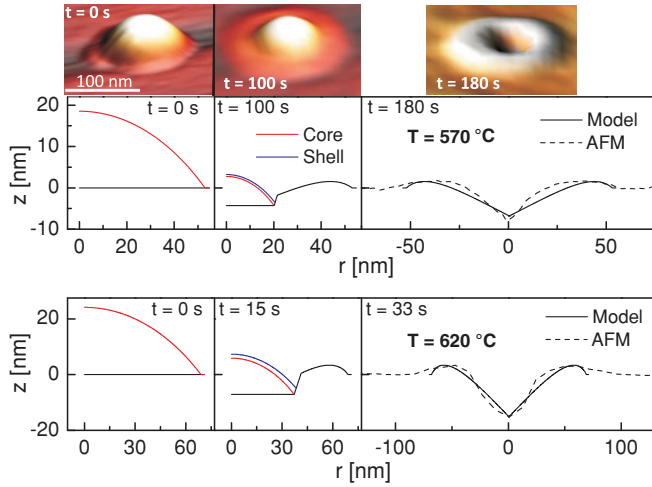
FIG. 4. (Color online) AFM images illustrating the transformation from droplets into holes with walls during annealing at $T = 570\,°C$ and annealing-time-dependent snapshots of the calculated droplet core (red), shell (blue), and substrate surface (black) morphologies at $T = 570\,°C$ and $T = 620\,°C$. Dashed lines represent AFM linescans of typical nanoholes fabricated at the process parameters of the calculations $\theta = 3.2$ ML.

the substrate surface

$$\frac{d}{dt}z = V_{GaAs}^{1/3} R_C. \tag{5}$$

Operationally, first the initial $N_{Ga,Core}$ is calculated from the temperature-dependent droplet density n and used as starting point for the time-dependent calculations. Now Eqs. (1) through (3) are iteratively solved yielding r_{Core}, r_{Shell} and with this the time dependent surface morphology via Eqs. (4) and (5).

The model considers four different processes and correspondingly four different rates and activation energies for Ga desorption E_D, substrate etching E_E, GaAs precipitation into the shell E_S, and wall deposition E_C as model parameters. To parametrize E_D, we refer to experimental data[14] revealing at $T = 570\,°C$ and $\theta = 3.2$ ML a critical time of about $t_c = 160$ s for the transformation from the droplets into holes. In the model, this critical time is represented by the instant at which $N_{Ga,Core}$ is reduced to less than one atom. Since the other parameters have an only negligible influence on t_c, this allows an unequivocal determination of $E_D = 2.35$ eV. For a fixed $E_S = 1.7$ eV, the value of $E_E = 1.895$ eV is identified by comparison with the experimental hole depth and the value of $E_C = 2.23$ eV by comparison with the wall height. The very good quantitative agreement of calculated and experimental surface morphologies for $T = 570$ and $620\,°C$ is demonstrated in Fig. 4.

VIII. MODEL RESULTS AND DISCUSSION

As a first important result, all calculations using the above parameters reveal that $x_{As,max} \gg x_{As} \simeq 0$ and $(A_{Core}/V_{GaAs}^{2/3})R_E \simeq (S_{Core}/V_{Ga}^{2/3})R_S$. This finding establishes that the desorption rate is high enough to yield immediate precipitation of all arsenic from the substrate into the shell. As
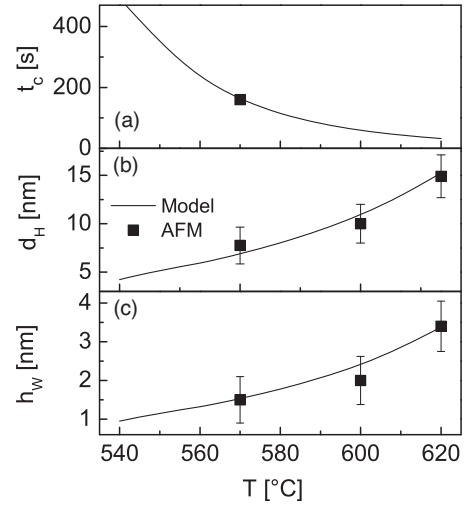

FIG. 5. Calculated and measured temperature dependence of (a) the critical time t_c up to hole formation, (b) the hole depth d_H, and (c) the wall height h_W.

a consequence, the shell formation process is governed by R_E and the rate R_S is not relevant. This allows the simplification of the above model and Eqs. (1) through (3) become now

$$\frac{d}{dt}N_{Ga,Core} = -\left(S_{Core}/V_{Ga}^{2/3}\right)R_D$$

$$N_{As,Core} = 0$$

$$\frac{d}{dt}N_{Shell} = \left(A_{Core}/V_{GaAs}^{2/3}\right)R_E - \left(A_{Shell}/V_{GaAs}^{2/3}\right)R_C.$$

The simplified model requires only three parameters E_D, E_E, and E_C. Using the above values, quantitative agreement with all results of the four-parameter model within the linewidth of the plots in Figs. 4 and 5 is achieved.

Figure 4 shows calculated snapshots of the transformation of the initial droplets into nanovulcanos during postgrowth annealing at $T = 570\,°C$ and $T = 620\,°C$. Clearly visible are the droplet shrinkage, the planar substrate material removal below the liquid droplet core, the formation of the GaAs shell, and the wall deposition. For illustration, additional AFM images of the different stages are shown for $T = 570\,°C$. Furthermore, Fig. 4(b) demonstrates the very good agreement between the calculated surface profiles and AFM linescans of typical nanoholes fabricated at the process parameters of the calculation.

Some additional points not directly visible in Fig. 4 are noted in the following. First, etching takes place until the droplet material has been completely removed and the droplet quasi sinks into the substrate during etching. Second, due to the with t reduced droplet volume and thus reduced r_{Core}, the surface area at which etching takes place becomes smaller with etching time. Third, since wall material is deposited only at the interface between droplet shell and substrate, with reduced droplet volume the surface area at which deposition takes place moves toward smaller radii. As a consequence, for small droplets, the shell does not further deposit material at the wall but instead refills the hole. Fourth, also the shell material is completely removed at the end of the etching process.

The temperature dependence of the critical time t_c up to hole formation, the hole depth d_H, and the wall height h_W is plotted in Fig. 5. Again, the model results agree very well with the experimental AFM data. As an important model result, for $T < 540\,°C$ the values of t_c become very long and etching freezes out. Furthermore, the data show that an increase of T yields an increase of both d_H as well as h_W. Incongruent evaporation limits the maximum temperature and, thus, the maximum hole depth to about 15 nm. Deeper holes with $d_H = 40$ nm can be achieved by etching with In droplets.[18] The surface morphology after In LDE at $T = 580\,°C$ is also quantitatively reproduced by the model if for the In-droplet density related characteristic energy $E_N = 2.21$ eV and for the etching activation energy $E_E = 1.87$ eV are used.

IX. CONCLUSION

In conclusion, a droplet core-shell model is suggested that represents the first quantitative description of the complex mechanism behind local droplet etching and wall formation. In particular, quantitative reproduction of experimental surface morphologies and the influence of the growth temperature is demonstrated.

[1] T. Chikyow and N. Koguchi, Jpn. J. Appl. Phys. **29**, L2093 (1990).

[2] J. H. Lee, Zh. M. Wang, E. S. Kim, N. Y. Kim, S. H. Park, and G. J. Salamo, Nanoscale Res. Lett. **5**, 308 (2010).

[3] T. Mano, K. Watanabe, S. Tsukamoto, N. Koguchi, H. Fujioka, M. Oshima, C. D. Lee, J. Y. Leem, H. J. Lee, and S. K. Noh, Appl. Phys. Lett. **76**, 3543 (2000).

[4] J. S. Kim and N. Koguchi, Appl. Phys. Lett. **85**, 5893 (2004).

[5] Ch. Heyn, A. Stemmann, A. Schramm, H. Welsch, W. Hansen, and A. Nemcsics, Phys. Rev. B **76**, 075317 (2007).

[6] M. Abbarchi, C. A. Mastrandrea, T. Kuroda, T. Mano, K. Sakoda, N. Koguchi, S. Sanguinetti, A. Vinattieri, and M. Gurioli, Phys. Rev. B **78**, 125321 (2008).

[7] E. Stock, T. Warming, I. Ostapenko, S. Rodt, A. Schliwa, J. A. Töfflinger, A. Lochmann, A. I. Toropov, S. A. Moshchenko, D. V. Dmitriev, V. A. Haisler, and D. Bimberg, Appl. Phys. Lett. **96**, 093112 (2010).

[8] M. Yamagiwa, T. Mano, T. Kuroda, T. Tateno, K. Sakoda, G. Kido, and N. Koguchi, Appl. Phys. Lett. **89**, 113115 (2006).

[9] T. Kuroda, T. Mano, T. Ochiai, S. Sanguinetti, K. Sakoda, G. Kido, and N. Koguchi, Phys. Rev B **72**, 205301 (2005).

[10] S. Huang, Z. Niu, Z. Fang, H. Ni, Z. Gong, and J. Xia, Appl. Phys. Lett. **89**, 031921 (2006).

[11] Ch. Heyn, A. Stemmann, and W. Hansen, Appl. Phys. Lett. **95**, 173110 (2009).

[12] Zh. M. Wang, B. L. Liang, K. A. Sablon, and G. J. Salamo, Appl. Phys. Lett. **90**, 113120 (2007).

[13] Ch. Heyn, A. Stemmann, R. Eiselt, and W. Hansen, J. Appl. Phys. **105**, 054316 (2009).

[14] Ch. Heyn, A. Stemmann, T. Köppen, Ch. Strelow, T. Kipp, S. Mendach, and W. Hansen, Appl. Phys. Lett. **94**, 183113 (2009).

[15] Ch. Heyn, A. Stemmann, T. Köppen, Ch. Strelow, T. Kipp, M. Grave, S. Mendach, and W. Hansen, Nanoscale Res. Lett. **5**, 576 (2010)

[16] Ch. Heyn, M. Klingbeil, Ch. Strelow, A. Stemmann, S. Mendach, and W. Hansen, Nanoscale Res. Lett. **5**, 1633 (2010).

[17] A. Stemmann, Ch. Heyn, T. Köppen, T. Kipp, and W. Hansen, Appl. Phys. Lett. **93**, 123108 (2008).

[18] A. Stemmann, Ch. Heyn, and W. Hansen, J. Appl. Phys. **106**, 064315 (2009).

[19] P. Alonso-González, D. Fuster, L. González, J. Martín-Sánchez, and Y. González, Appl. Phys. Lett. **93**, 183106 (2008).

[20] J. Tersoff, D. E. Jesson, and W. X. Tang, Science **324**, 236 (2009).

[21] D. P. Kumah, S. Shusterman, Y. Paltiel, Y. Yacoby, and R. Clarke, Nature Nanotechnology **4**, 835 (2009)

[22] S. Clarke and D. D. Vvedensky, Phys. Rev. Lett. **58**, 2235 (1987).

[23] C. D. Thurmond, J. Phys. Chem. Solids **26**, 785 (1965).

[24] W. Ostwald, Z. Phys. Chem. **34**, 495 (1900).